Morphological Properties of Flocs Under Turbulent Break-Up and Restructuring Processes

M. Vlieghe
Laboratoire de Génie Chimique, Université de Toulouse, CNRS, INPT, UPS, Toulouse, France

LISBP, Université de Toulouse, CNRS, INRA, INSA, Toulouse, France

C. Frances and C. Coufort-Saudejaud
Laboratoire de Génie Chimique, Université de Toulouse, CNRS, INPT, UPS, Toulouse, France

A. Liné
LISBP, Université de Toulouse, CNRS, INRA, INSA, Toulouse, France

Bentonite flocculation was performed in a Taylor–Couette reactor coupled with an in situ method of image acquisition and analysis. A hydrodynamic sequencing is imposed to perform successive cycles of flocculation and breakage. Depending on the shear rate applied during the breakage step, one or two cycles are needed after the first flocculation step to recover a full reversibility on both size and shape factors. The breakup step produces flocculi that are the build-ing blocks for the next. The re-flocculation steps produce smaller sizes and more regular shapes than the initial growth step. The floc size is calibrated by the turbulence as the radius of gyration is close to the Kolmogorov microscale whereas the floc structure is determined by flocculi aggregates. An analysis of the change of the flocs morphology, despite of their diversity, can also be achieved thanks to some relevant moments of the distributions.
Keywords: Taylor–Couette reactor, flocculation, aggregation, break-up, morphology

Introduction

A wide variety of particulate processes deal with suspended particles in fluids (precipitation or synthesis processes, wet grinding, flocculation, solid–liquid mixing or product formulation, . . .). The population of suspended material, composed of particles, aggregates or flocs, is characterized by a distribution usually defined with respect to the mass, the volume, a characteristic dimension of the particle or the number of primary entities inside the aggregate. The morphological and structural properties also play an important role on the end-use properties (catalytic, shape, or texture properties), or their flowing behavior (viscosity, sedimentation). For these reasons, it is often important to analyze the effect of hydrodynamic conditions on the whole size and shape properties; this last one being described at several scales, from the local one (structure, porosity) to a more global one (silhouette, aspect ratio, circularity, . . .).

The structural properties of aggregates or flocs are currently described by a fractal dimension representative of the whole population.[1–3] Many other morphological properties may be extracted from image analysis, allowing characterizing the global shape of the aggregates, such as the aspect ratio[4–6] or the elongation.[7] The presence of concavities (solidity),[8,9] the surface roughness (convexity)[8,10] or the circularity which is sensitive to both the global and local shapes[11,12] may also be calculated from image analysis as well as a 2D fractal dimension linking the floc area to the perimeter or to a floc size.[7,13]

A focus is done in this article on the flocculation process which is commonly used for example in drinkable water production. During this process, the aggregation of fine particles suspended in water is enhanced by the addition of a coagulant; particle aggregation allows their further separation by filtration or decantation. This operation is usually done under turbulent hydrodynamic conditions to promote the mixing and the collision of particles which encounter to form flocs. But the hydrodynamic conditions also induce floc breakage or compaction, limiting the growth of aggregates. During the first period of the flocculation process, the size of flocs increases rapidly but then the breakage phenomena take place which counteract the aggregation process and a stationary state is reached.[14–16] The floc sizes obtained at steady state are highly correlated with the hydrodynamic conditions usually expressed by the mean shear rate G (s^{-1}). Higher is G, smaller are the flocs. Many experimental works of the literature[17] indicate a proportionality between the size and $G^{-1/2}$ or directly with the Kolmogorov microscale[4,15,18,19] η, both expressions being equivalent. Sometimes a decrease of the size is observed before reaching

Correspondence concerning this article should be addressed to C. Frances at Christine.Frances@ensiacet.fr.

the steady state suggesting the existence of breakage or restructuring phenomena[20–24].

A sequence of the hydrodynamic conditions, applying alternative steps at low and high shear rates is performed to characterize the effect of hydrodynamics on the floc properties taking into account their history. Indeed, performing a cycle sequence comprising three phases (flocculation/breakage/re-flocculation), François[25] put in evidence the non-reversibility of the process. The sizes of floc produced by re-flocculation were smaller than the ones produced during the first flocculation phase. The flocs obtained during the breakage step were also smaller if the shear rate applied is higher. Such a behavior was explained by the multi-scale structure of flocs: the primary particles bond each other to form small aggregates (flocculi) which themselves stick to each other to produce larger aggregates and flocs. Other papers report the same behavior concerning bentonite,[26–28] kaolin,[29] or humic acid.[30,31]

Moreover, concerning the structure of flocs, several authors have observed a change of the fractal dimension during the growth phase of a flocculation process, indicating the formation of open and irregular structures poorly compacted. The value of the fractal dimension itself, regardless of the definition used, varies with the nature of the material and the flocculation mechanism.[28,32] When a shear rate is applied, the fractal dimension may change depending on the floc strength and the breakage mechanism.[24]

The change of the dispersed medium thus results from a competition between the aggregation, breakage and restructuring phenomena which all depend on the solid properties, the physico-chemical conditions and the hydrodynamic conditions. In this context, the *in situ* simultaneous analysis of size and shape properties of mineral flocs under controlled hydrodynamic conditions could bring a better understanding of the flocculation process. In this study the physico-chemical properties will be fixed, a focus will be made on the effect of the hydrodynamic conditions on the morphological properties of flocs.

This article presents the results of an experimental work on the flocculation of bentonite performed under turbulent conditions in a Taylor–Couette reactor. A sequence of the hydrodynamic conditions is applied to analyze the change of the morphological properties and their reversibility over successive cycles.

Experimental Set-Up and Validation Analysis

Materials and methods

A natural clay (bentonite), supplied by CECA Chemicals was used in this study as a model material due to its properties similar to those of the materials usually encountered in drinkable water resources (rivers). The particles of bentonite dispersed in water are structured as small aggregates of a few microns in size constituted by platelets of a ten of nanometers, resulting themselves from the pile of primary sheets having a thickness of about one nanometer.[33] The experiments were done at a fixed bentonite mass concentration of 30 mg L^{-1} suspended in demineralized water. To avoid any disturbance due to the swelling ability of bentonite, the suspension was prepared long before the experiments. Aluminum sulfate hydrate with the formula $\left(Al_2(SO_4)_3 \cdot 14H_2O\right)$ was chosen as a coagulant, and prepared at an appropriate concentration to get a fixed concentration of 3.5×10^{-5} mol L^{-1} after dilution of 5 mL of the aluminum sulfate solution into the bentonite suspension. The pH of the resulting suspension was equal to 4.5 ± 0.1, ensuring the main presence of Al^{3+} ions and allowing a coagulation mechanism by charge neutralization.[34]

The experiments were performed in a Taylor–Couette reactor constituted by two concentric cylinders of a height of 20 cm. The outer cylinder of a radius $R_{ext}=11.5$ cm is at rest while the inner cylinder of a radius $R_{int}=10$ cm rotates at a chosen angular velocity Ω. The volume of the separation gap is equal to 2 L.

In the Taylor–Couette geometry, the dimensionless number which defines the flow type is the Taylor number which compares centrifugal inertia forces and viscous forces:

$$Ta=\frac{R_{int}\Omega^2(R_{\text{ext}}-R_{int})^3}{v^2} \tag{1}$$

where Ω (rad s^{-1}) is the angular velocity of the inner cylinder and v the suspension kinematic viscosity (m^2 s^{-1}).

Moreover, the mean velocity gradient is defined by:

$$\langle G\rangle=\sqrt{\frac{P}{\rho v\ V}} \tag{2}$$

where V is the volume of the reactor (m^3), ρ the suspension density (kg m^{-3}), and P (Watt) the global power dissipated in the reactor function of the torque and the angular velocity, given by Wendt.[35] The dissipated power is also related to the mean dissipation rate of the turbulent kinetic energy $\langle\varepsilon\rangle$ (m^2 s^{-3}) by:

$$\langle\varepsilon\rangle=\frac{P}{\rho V} \tag{3}$$

And thus:

$$\langle G\rangle=\sqrt{\frac{\langle\varepsilon\rangle}{v}} \tag{4}$$

In the case of isotropic turbulence, the mean Kolmogorov microscale, which has a great importance in flocculation analysis as indicated above, can be estimated from the mean dissipation rate by:

$$\langle\eta\rangle=\left(\frac{v^3}{\langle\varepsilon\rangle}\right)^{1/4} \tag{5}$$

Floc characteristics were acquired through image processing. It consists in the capture of images using a CDD camera (FlowSense EO 16M), synchronized with a laser sheet (Nd : Yag 532 nm, 30 mJ) illuminating a tangential plane with a thickness of about one millimeter at the middle distance in the gap between the cylinders. Grayscale images with a spatial resolution 4872×3248 $pixels^2$ were taken at a frequency of 4 Hz. To reduce refraction effect through the outer cylinder walls, the Taylor–Couette reactor was enclosed within a cubic box made of Plexiglas and filled with glycerol, both having close refractive indexes. Special attention was paid on particle image treatment to isolate individual flocs and get high quality binarized images applying a gray level threshold. Details of the image processing can be found in Vlieghe et al.[36] Binarized images were then analyzed using the Matlab function named "regionprops." Several size and shape properties can be directly determined as the perimeter, area, circle equivalent diameter, ... etc. and other morphological parameters, such as circularity, convexity, solidity, ... can also be derived from the previous ones. However many descriptors give redundant

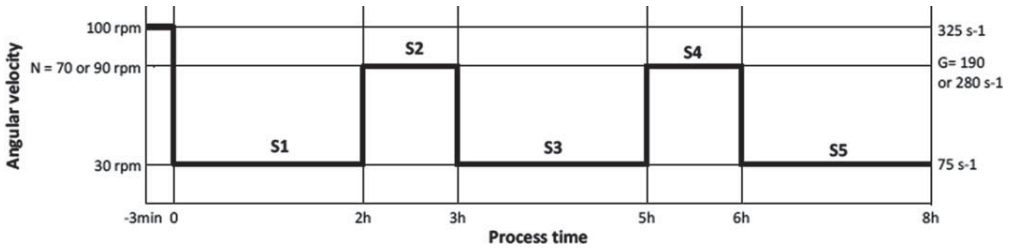

Figure 1. Experimental protocol.

information and some of them are more relevant than the others. The radius of gyration and the circularity were chosen here since they were shown, respectively, as relevant size and shape properties to characterize bentonite floc size and shape.[36] Let's remember that the radius of gyration is a size property calculated by:

$$R_g^2 = \frac{1}{A_p}\sum_{i=1}^{A_p}\left[(x_i - x_c)^2 + (y_i - y_c)^2\right] \quad (6)$$

where A_p is the number of pixels on the image of the aggregate, (x_i, y_i) the pixel coordinates, and (x_c, y_c) the centroid coordinates.

The circularity is defined as the ratio of the circle equivalent perimeter to the actual perimeter:

$$C_i = \frac{\sqrt{4\pi A}}{P} \quad (7)$$

The circularity may vary between 0 and 1; it is an indicator of the overall shape as well as the boundary roughness of the floc.

Precisions on experimental protocol and analysis

Sequenced flocculation runs were performed to analyze the aggregation, break-up and re-structuring processes. During the experiments, the Taylor–Couette reactor is first filled with the bentonite suspension and the inner cylinder rotation is switched on at 100 rpm. The flocculent is then added with a 5 mL calibrated pipette in the separation gap halfway-up the reactor. A 3-min step at a high rotating velocity ($N = 100$ rpm) is then applied to promote a rapid mixing of the suspension with the solution of coagulant and to allow the collision of single particles the ones to the others leading to the formation of the first aggregates.

Then alternative steps at low and high shear rates are imposed as illustrated on Figure 1 allowing the aggregation and the breakage of flocs. The growth of flocs is thus promoted when a low shear rate is applied. During these steps, named "aggregation steps" (steps S1, S3, S5) in the following sections, the shear rate was fixed at 75 s^{-1} (which corresponds to an angular velocity $N = 30$ rpm) and maintained at this rate during two hours. The breakage of flocs is then promoted increasing the shear rate, even if aggregates can still be formed during this period. The duration of these steps, named "breakage steps" (steps S2, S4) was fixed at one hour and the shear rate applied was maintained constant at 280 s^{-1} ($N = 90$ rpm) for the Run 1 or 190 s^{-1} ($N = 70$ rpm) for the Run 2. The flow characteristics as defined by Eqs. 1–5 corresponding to the global hydrodynamic conditions imposed during the experiments are reported on Table 1. Since the experiments were conducted in diluted conditions, the suspension properties were assumed to be identical to those of water. Whatever the conditions imposed during the sequenced flocculation process, the hydrodynamic regime corresponds to turbulent Taylor vortex flow.

Several experiments were conducted under the same conditions to evaluate the reproducibility of the results. It was fairly good both on the number-based and surface-based distributions of any size or shape parameters obtained at the end of each cycle sequence. For example the error (in a log-scale) of the modes of the area distribution calculated on images of flocs both on a surface or a number base was less than 2.5%. The errors on the modes of the perimeter distribution never exceed 3.5%. As an illustration, the surface-based and the number-based perimeter distributions obtained at steady state after the first cycle sequence of breakage (S2) are, respectively, reported on Supporting Information (see Figures 10a, b).

However, to ensure a relevant morphological characterization, only floc images composed of 10 pixels or more were taken into account, thus the smallest aggregates analyzed have a circle equivalent diameter of 26 μm and the minimum radius of gyration considered is 9 μm. This treatment mainly affects the number of flocs considered for the analysis. Depending on measurements, between 50 and 65% of the detected areas are eliminated. They correspond to isolated pixels related to the imprecision of the background as well as to small flocs. Despite of this treatment, the number of flocs analyzed is always greater than 60,000.

Due to this procedure, some small flocs, mainly produced during the breakage steps (or not destabilized) and having a size less than 10 pixels are not taken into account in the results. The mass of the sample analyzed from one step to the other is thus not strictly conserved. However, since the eliminated areas are less than 10 pixels, the cumulated area is only a little bit affected during this treatment (less than 5%). Meanwhile, the cumulated perimeter is reduced of 15%. But the trends on the cumulated parameters, such as the number, the area or the perimeter calculated on the raw data or on the modified ones neglecting areas less than 10 pixels, are very similar (see Supporting Information Figures 11a–c). So, this image analysis procedure can adequately characterize the morphological properties of flocs and be used for comparison

Table 1. Global Hydrodynamic Characteristics of the Taylor–Couette Reactor

N (rpm)	30	70	90	100
Ta (–)	3.3×10^6	1.8×10^7	3.0×10^7	3.7×10^7
ε ($m^2 s^{-3}$)	5.4×10^{-3}	37×10^{-3}	77×10^{-3}	106×10^{-3}
G (s^{-1})	75	190	280	325
η (μm)	116	72	60	55

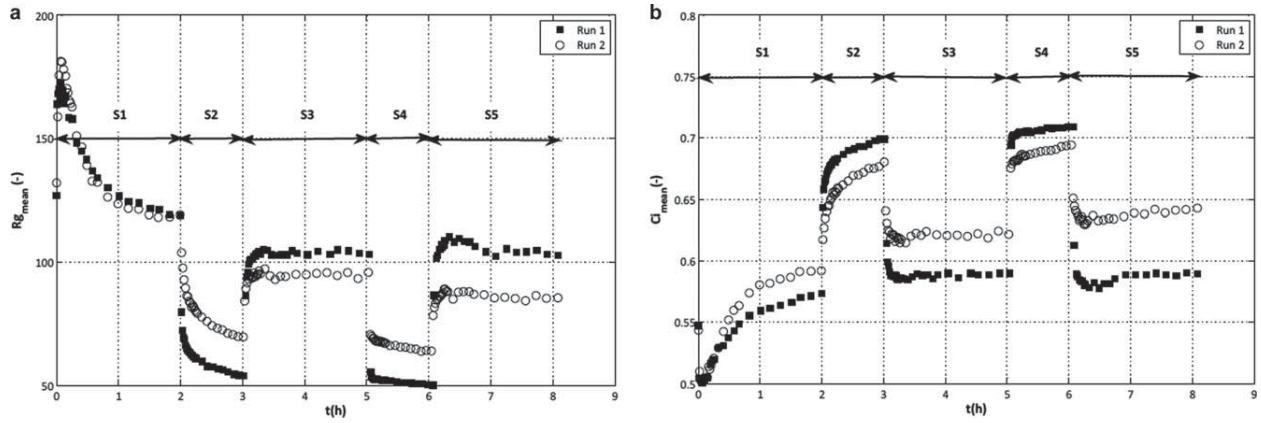

Figure 2. (a) Change of the surface-based mean radius of gyration vs. time over the different steps. (b) Change of the surface-based mean circularity vs. time over the different steps.

purposes. An increase of the number of flocs results from the preponderance of the breakage mechanism (steps S2 and S4) over the aggregation one (steps S1, S3 and S5). Inversely, a decrease of the number of flocs expresses the preponderance of aggregation. Similarly, an increase of the cumulated perimeter corresponds to the breakage of flocs, while a decrease indicates a preponderance of the aggregation mechanism or a significant restructuring phenomenon. Finally, an increase (resp. a decrease) of the cumulated apparent area, which can be seen in a 3D-view as an apparent volume, results from an increase of the porosity (resp. a floc compaction) as far as the mass is conserved.

Results and Discussion

Surface-based mean floc characteristics over the different flocculation steps

The results are first analyzed with respect to the mean floc characteristics. The changes of the surface-based mean gyration radius and the surface-based mean circularity vs. time are, respectively, reported on Figures 2a, b. The corresponding relative standard deviations (ratio of the standard deviation on the mean property) for the radius of gyration and the circularity are reported on the paper on-line version (see Supporting Information Figures 12a, b).

Opposite trends are observed on Figure 2a compared to Figure 2b all along the different phases. Moreover, the change corresponding to Run 1 ($\langle G\rangle = 280\ s^{-1}$) and Run 2 ($\langle G\rangle = 190\ s^{-1}$) are similar but the amplitude is more important for the Run 1, for which the gap between the shear stress for two consecutive steps if higher.

During the first phase (S1), the mean radius of gyration sharply increases during the first minutes, as flocs are formed, and then slowly decreases meanwhile a re-structuration of flocs occurs (cf. Figure 2a). When the flocs are formed by aggregation, the change of the standard deviation over time (see Figure 12a) reveals that the distribution of flocs rapidly spreads over time first and then it decreases indicating a homogenization of the population. Indeed it was pointed out on previously that during this change the floc number and the cumulative perimeter increase whereas the apparent total area slightly decreases; all of this being coherent with a breakage mechanism and finally a floc compaction vs. time. Symmetrically, the floc circularity strongly decreases first and then slowly increases during the first phase (Figure 2b). The decrease of the relative standard deviation (see Figure 12b) during the first aggregation step is also consistent with a restructuration of the system.

On the base of the evolution of the floc size and shape distributions (not reported here), it was concluded that a steady state was reached after about two hours. The stress conditions imposed during the first phase are the same for the two runs. As expected, the mean radii of gyration are quite similar. However it can be observed on Figure 2b that the mean circularity differs significantly. This difference can only be attributed to the poor reproducibility of the results during this first phase as it was reported before.

During the second phase (S2) and the fourth as well (S4), corresponding mainly to breakage due to an increase of the shear stress, the mean radius of gyration (Figure 2a) strongly decreases whereas the circularity increases (Figure 2b). The breakage steps S2 and S4 also lead to a decrease of the relative standard deviation (see Figures 12a, b in the Supporting Information) showing that the population is more homogeneous in size and shape. The changes vs. time during the two steps are rather similar. However the steady state is not reached after one hour during S2, whereas the mean values of the two characteristic parameters do not evolve any more after 1 h during the step S4. The process time-scale can be evaluated fitting the mean parameter vs. time with an exponential decreasing law. Thus, the breakage kinetics is more rapid for the step S4 compared to the step S2 with a reduction of the breakage time-scale from approximately 3 to 2 min for the Run 1 ($\langle G\rangle = 280\ s^{-1}$) and from 11 to 7 minutes for the Run 2 ($\langle G\rangle = 190\ s^{-1}$). The structuration induced by the hydrodynamic conditions during S4 leads to more compact flocs, having a mean size slightly smaller (and a circularity slightly higher) than those produced at the end of S2. Moreover, the breakage steps imposed during the Run 1 produce flocs having a mean size clearly smaller (30%) than those produced during the Run 2, but the floc shape is nearly the same.

The third and the fifth phase (S3 and S5) mainly correspond to an aggregation mechanism due to a low shear stress as for the first phase. However, the initial population is not the same; it corresponds to the population created during the previous breakage step for S3 and S5 whereas it was composed by initial aggregates for the phase S1. As a consequence, the growth is very rapid during the phases S3 and S5 with a reduction of the aggregation time-scale from 1.5 to 0.9 min for the Run 1 ($\langle G\rangle = 280\ s^{-1}$) between the two steps and about 2 min for

both steps for the Run 2 ($\langle G\rangle = 190\ s^{-1}$). The mean radius of gyration of flocs produced during S3 (around 103 μm for Run1 and 96 μm for Run 2) and S5 (around 103 μm for Run1 and 86 μm for Run2) is smaller than during S1(119 μm for both runs). Concerning the shape change, it can be observed on Figure 2b that the mean circularity rapidly decreases during the steps S3 and S5 and then tends to a stationary and identical value. The re-flocculation steps S3 and S5 generate a variety of shapes. Thus, the population of flocs is more heterogeneous and the relative standard deviation gets higher values. This effect is more pronounced for the Run 1.

Moreover, the flocs produced during the re-flocculation steps (S3 and S5) are larger for the Run 1 ($\langle G\rangle = 280\ s^{-1}$) than for the Run 2 ($\langle G\rangle = 190\ s^{-1}$). The initial aggregates produce during the corresponding breakage steps (S2 and S4) are smaller for the Run 1 (higher shear stress) and this seems to promote aggregation. During the runs, a slight re-structuration can be observed. It can above all be observed during the step S5 for the Run 1. Indeed, the growth first and then the breakage and the re-structuration can only occur if the initial flocs are small enough. For the Run 1, the final state reached during S5 seems to be identical to the one observed at the end of the step S3. On the opposite, for the Run 2, the aggregates formed during S5 are more rounded (having a smaller size and a higher circularity) than those formed during S3.

To get more quantified information on the reversibility of the process over the hydrodynamic sequencing, several ratios based on the mean properties may be used. For example, the strength factor (SF) and the recovery factor (RF) as defined by François[25] may be applied both on the breakage and re-flocculation phases. SF is a measure of the floc strength property and RF quantifies the reversibility of the size change. These factors have been calculated on the base of the mean radius of gyration obtained at the end of each phase by the following expressions:

$$SF = \frac{Rg_B}{Rg_{A1}} \tag{8}$$

$$RF = \frac{Rg_{A2} - Rg_B}{Rg_{A1} - Rg_B} \tag{9}$$

where Rg_B is the mean radius of gyration of flocs at the end of a breakage step (S2 or S4), and Rg_{A1} (respectively, Rg_{A2}), the mean radius of gyration after a first flocculation step (S1 or S3) (respectively, a second flocculation step S3 or S5).

Similar analysis can be done considering the mean circularity values and thus defining the circularity factor (CF) which characterizes the floc compaction and the recovery shape factor (RSF) which expresses the reversibility of the shape property as:

$$CF = \frac{Ci_B}{Ci_{A1}} \tag{10}$$

$$RSF = \frac{Ci_{A2} - Ci_B}{Ci_{A1} - Ci_B} \tag{11}$$

where Cig_B is the mean circularity of flocs at the end of a breakage step (S2 or S4), and Ci_{A1} (respectively, Ci_{A2}), the mean radius of gyration after a first flocculation step (S1 or S3) (respectively, a second flocculation step S3 or S5).

The numerical values of the mean properties at the end of each phase, as well as the different factors calculated by Eqs. 8–11 are reported on Table 2.

Between the first and the second breakage cycle, the strength factor increases and the floc compaction is slightly reduced. The strength factor is also obviously higher and the compaction lower for the Run 2 ($\langle G\rangle = 190\ s^{-1}$) compared to Run 1 ($\langle G\rangle = 280\ s^{-1}$). The ability of breakage is higher when the stress conditions are more severe and the aggregates are thus more rounded. Moreover a full reproducibility on both size and shape factors is observed during the second cycle on Run 1 (*RF(S4)* and *RSF(S4) = 1*). A longer phase duration or another breakage/re-flocculation cycle would have been necessary to recover perfect reversibility when soft stress conditions (as for Run 2) are applied.

Table 2. Reported Values of the Mean Properties of Flocs at the End of Each Step: (a) Radius of Gyration; (b) Circularity

	Run 1 $G = 280\ s^{-1}$	Run 2 $G = 190\ s^{-1}$	Gap %
(a) Rg_{mean}(μm) at the end of the cycle			
S1	118.9	119.0	0.1
S2	53.7	69.6	29.6
S3	103.2	95.8	7.7
S4	50.1	63.9	27.5
S5	102.9	85.5	20.3
Characteristic ratios			
SF(S2)	0.45	0.58	
SF(S4)	0.49	0.67	
RF(S2)	0.76	0.53	
RF(S4)	0.99	0.68	
(b) Ci_{mean}(–) at the end of the cycle			
S1	0.57	0.59	3.3
S2	0.70	0.68	2.8
S3	0.59	0.62	5.4
S4	0.71	0.69	2.2
S5	0.59	0.64	9.2
Characteristic ratios			
CF(S2)	1.22	1.15	
CF(S4)	1.20	1.12	
RSF(S2)	0.87	0.66	
RSF(S4)	1.00	0.71	

Steady state distributions of floc properties

Here are analyzed the size distributions obtained after each phase under different stress conditions. The surfaced-based size distributions (with respect to the radius of gyration) and the number-based size distributions are plotted on Figures 3a, b for the Run 1 ($\langle G\rangle = 280\ s^{-1}$) and Figures 4a, b for the Run 2 ($\langle G\rangle = 190\ s^{-1}$).

It is clear on Figures 3a, b and 4a, b that the surface-based distributions are monomodal whereas the number-based distributions are multimodal, characterized by an important population of very small particles and one or even two other populations of larger flocs. The fine sub-population does not evolve during the different steps, indicating that this population, mainly constituted by the initial particles or very small aggregates, is not destabilized by salt addition. Let's now compare the distributions obtained for these two runs. A clear distinction between the aggregation and breakage phases can be done for the Run 1 ($\langle G\rangle = 280\ s^{-1}$). This difference is less pronounced for the second run; the flocs produced during the aggregation phases being smaller and those formed during the breakage steps being larger. For both runs, the size distributions at the end of the breakage steps (S2 and S4) are close to each other but not perfectly superimposed. The surface-based distributions slightly move toward smaller sizes in agreement with the observations done previously on the mean values.

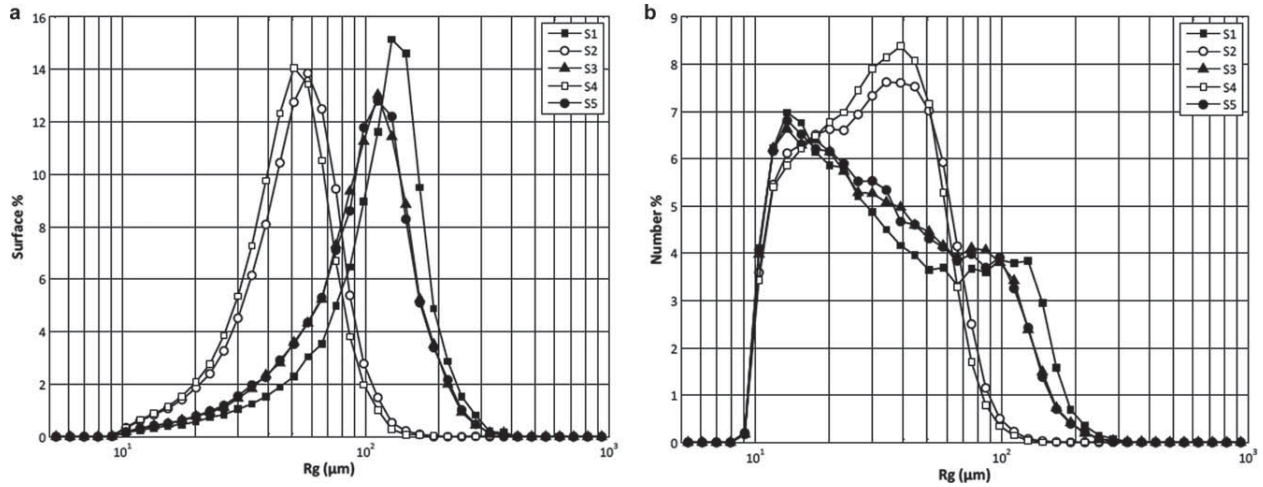

Figure 3. (a) Surface-based gyration radius distributions for the different steps—Run 1($\langle G \rangle$=280 s^{-1}). (b) Number-based gyration radius distributions for the different steps—Run 1 ($\langle G \rangle$=280 s^{-1}).

Looking at the number-based distributions, it can be see that the mode of the main population is the same (around 39 μm for the Run 1 and 44 μm for the Run 2) for the steps S2 and S4, only the maximum size and the proportion of larger flocs are different for these two breakage steps. It may be assumed that the flocs are calibrated by the hydrodynamics conditions and this process initiated during S2 continues during S4. Stationary identical states could probably be achieved with a longer breakage phase duration.

Concerning the re-flocculation steps, the size distributions recovered at the end of the steps S3 and S5 are well superimposed (both on surface-based and number-based distributions) for the Run 1 ($\langle G \rangle$=280 s^{-1}) which can thus be assumed as fully reproducible, whereas the aggregation mechanism during the Run 2 ($\langle G \rangle$=190 s^{-1}) is only partially reversible. Moreover, the number-based distributions allow observing the presence on the curves associated with the re-flocculation steps S3 and S5 of a sub-population corresponding to the primary mode of flocs produced during the previous breakage steps (around 39 μm for the Run 1 and 44μm for the Run 2). This is more obvious for the Run 2, for which trimodal distributions are obtained, constituted by passive primary aggregates (mode around 12 μm), small flocs resulting of the breakage step (mode around 44 μm) and large flocs obtained by aggregation (mode around 75 μm).

As depicted in the introduction, the effect of the hydrodynamic conditions on the floc size can be interpreted on the base of the viscous dissipation of the kinetic energy occurring at the Kolmogorov micro-scale. Here, the mean Kolmogorov calculated for the different shear rates imposed during the cycle sequence: ($\langle G \rangle$=75 s^{-1}) for the aggregation steps, ($\langle G \rangle$=280 s^{-1}—Run 1) on one hand and ($\langle G \rangle$=190 s^{-1}—Run 2) on a second hand for the breakage steps has been compared on Figure 5 to the mode of the related floc size distributions.

All along the flocculation sequence, the flocs mainly have a size close to the mean Kolmogorov micro-scale, indicating that the flocs produced under a shear rate are calibrated by the Kolmogorov microscale in agreement with previous results of the literature. Concerning the breakage steps (S2 and S4), the floc characteristic diameter (mode of the Rg distributions) remains close to the mean Kolmogorov microscale although it

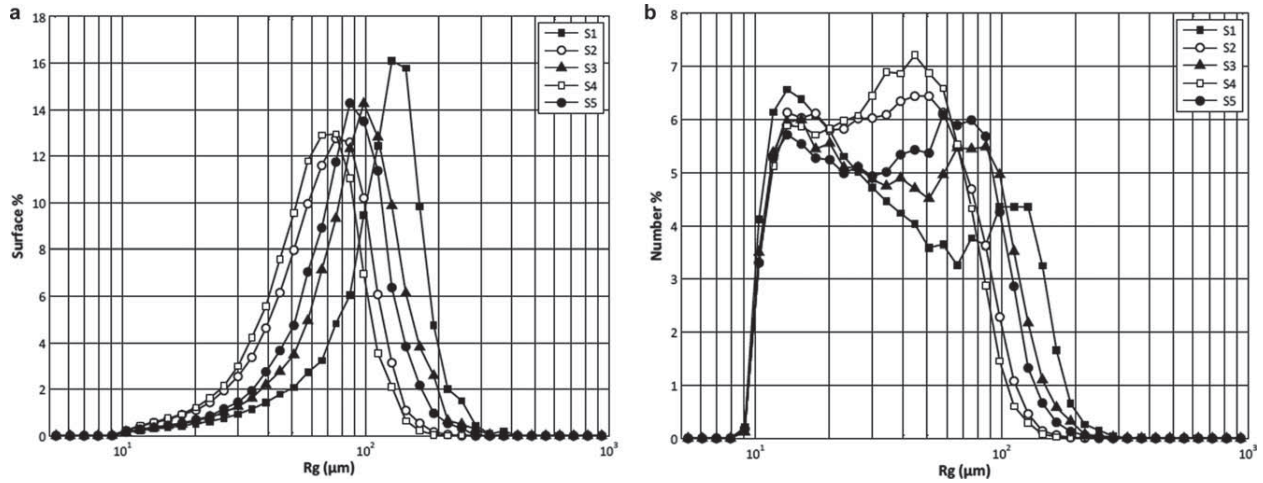

Figure 4. (a) Surface-based gyration radius distributions for the different steps—Run 2 ($\langle G \rangle$=190 s^{-1}). (b) Number-based gyration radius distributions for the different steps—Run 2 ($\langle G \rangle$=190 s^{-1}).

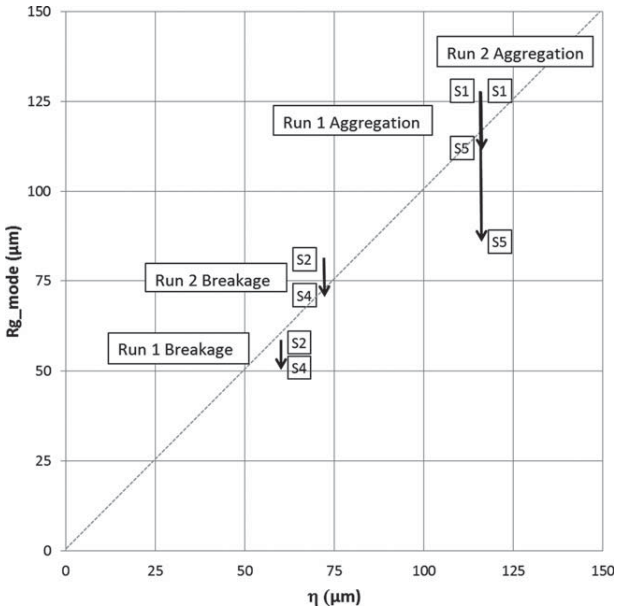

Figure 5. Comparison of the floc size with the Kolmogorov micro-scale.

is slightly reduced between the two cycle sequences. The characteristic size corresponding to the flocs produced during the first aggregation step (step S1) is higher than the mean Kolmogorov microscale. But it decreases then for the following re-flocculation steps (S3 and S5), and becomes lower than the mean microscale, especially for the Run 2. Let's remember that the hydrodynamics in the Taylor–Couette is heterogeneous showing more or less stressing conditions depending on the zones of the reactor; the more intense being is in the wall regions and the less one in the center of the toroidal vortices. So large flocs may be formed in the regions where the stress conditions are the softest and be broken when they pass through the zones where the stress conditions are harder.

We consider now the circularity distributions obtained at steady state for the different phases and runs. The surface-based and number-based circularity distributions are, respectively, reported on Figures 6a, b for the Run 1($\langle G\rangle = 280\ s^{-1}$) and Figures 7a, b for the Run 2 ($\langle G\rangle = 190\ s^{-1}$).

Contrary to the size distributions, both the surface-based and the number-based circularity distributions are monomodal. For both experiments, the distributions corresponding to the breakage steps (S2 and S4) are close, the circularities being slightly higher at the end of the step S4. Moreover the number and surface distributions are very similar. The effect of size in correlation with the type of representation is not significant (the surface distribution putting in evidence the property of the coarser fraction compared to the number distribution). The similarity between the two types of representation suggests that all the sub-populations, distinguishable by their size, present the same variety of shape. On the contrary the flocs produced during the aggregation steps, especially during the first step (S1) have different distributions depending on the type of representation. The effect of size correlated with the type of representation is now significant. Although the initial population or the flocs produced during the breakage steps have similar size and shape, the large flocs appeared during the aggregation phases lead to a variety of shapes. The range of variation of the circularity is increased on the left hand side of the curves (less circular flocs are created). This effect is clearly seen on the surface distributions, but also on the number distributions. For the Run 1, the circularity distributions after the three aggregation phases are rather similar. This is not surprising since the hydrodynamic conditions which produced the initial flocs were close (100 rpm during the coagulation phase before the step S1, compared to 90 rpm for the breakage steps before the re-flocculation phases). On the contrary for the Run 2, the initial flocs for the re-flocculation steps S3 and S5 (produced at 75 rpm) are different to those forming the initial population for the step S1. Finally, if soft conditions are applied during the breakage steps, the initial flocs for the aggregation phase are larger and they give birth to smaller flocs, less complex (more rounded flocs having a higher circularity).

Quantitative Analysis of Populations During the Flocculation Steps

In this section, attention is paid on the shape of the distributions. It is often convenient to compare the distribution of a population with some classical ones, as the normal or the log-normal distributions. This can be easily done calculating selected parameters derived from some specific moments of the distribution. The first raw moment (m_1) taking into

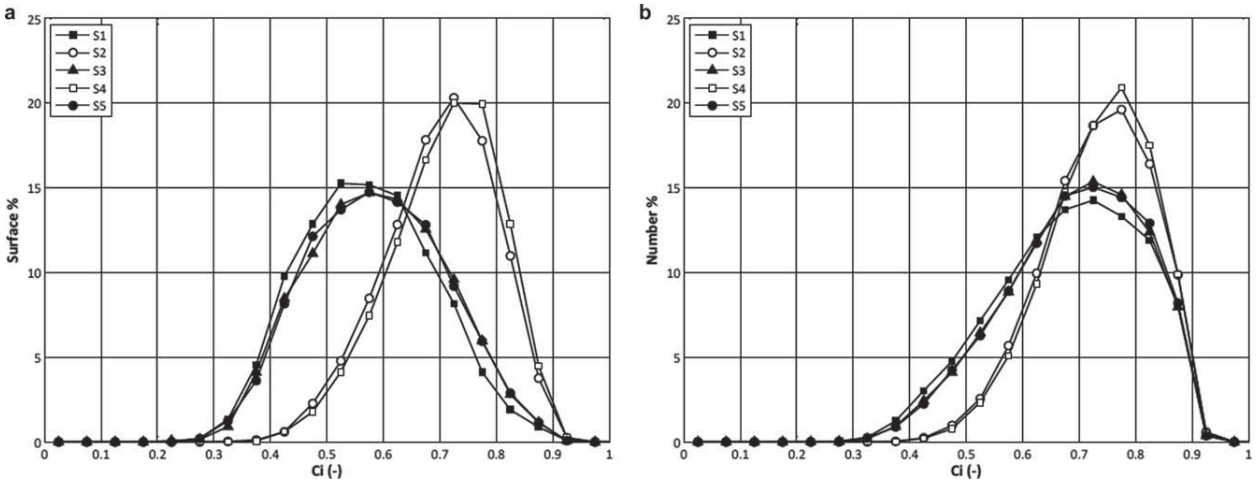

Figure 6. (a) Surface-based circularity distributions for the different steps ($\langle G\rangle = 280\ s^{-1}$—Run 1). (b) Number-based circularity distributions for the different steps ($\langle G\rangle = 280\ s^{-1}$—Run 1).

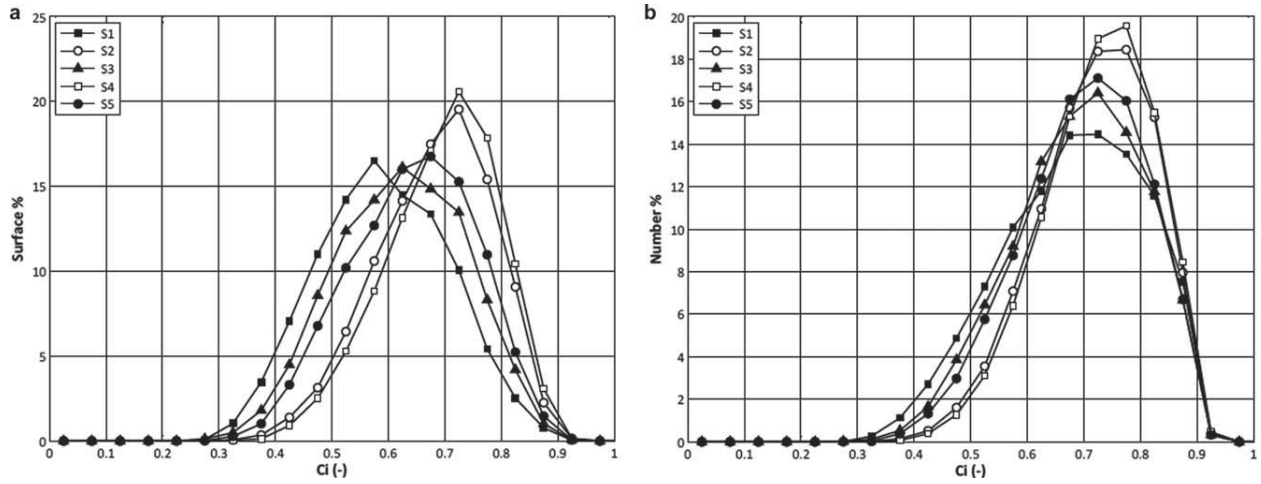

Figure 7. (a) Surface-based circularity distributions for the different steps ($\langle G \rangle$=190 s^{-1}—Run 2). (b) Number-based circularity distributions for the different steps ($\langle G \rangle$=190 s^{-1}—Run 2).

account the floc surface represents the surface mean, as reported on Figures 2a, b. The standard deviation (σ) of the surface-based distribution is the positive square root of the second central moment. The moments of the distributions were calculated directly from the experimental data measured on several thousands of individual flocs.

Since the distributions of the radius of gyration are plotted on a log-scale, it is more relevant to compare them to a log-normal distribution. For that purpose, the moments of the steady state distributions of Rg in log-scale were calculated allowing the determination of the two characteristic parameters μ_{Rg} and σ_{Rg} of the log-normal law (see Table 3a). The theoretical log-normal distributions were then compared to the experimental distributions of the radius of gyration. An illustration is given in the Supporting Information (Figure 13a) for the Run 1. Similar results were obtained for the Run 2 (not reported here). It is obvious that log-normal laws cannot properly fit the experimental size distributions. The general trend of the curves is well simulated but the theoretical laws underestimate the amount of small aggregates on the left part of the curves. The modes of the distributions are lower than the experimental modes and the maximum surface percentages are also underestimated.

The same analysis was done for the circularity distributions, excepted that they were compared to normal laws. The corresponding values of the characteristic parameters μ_{Ci} and σ_{Ci} of the normal law are reported on Table 3b. A comparison with the experimental distributions is reported on the Supporting Information (Figure 13b) for Run 1. The same observations were done for the Run 2. The experimental circularity distributions are better predicted by normal laws than previously but the curves are not perfectly fitted.

Additionally, some other moments of the distributions can be used to refine the analysis. Indeed, the skewness (s), which indicates if a distribution is symmetric or has a tail on the left or the right side, is the normalized third central moment and the kurtosis (or excess kurtosis) ($\kappa - 3$) which is a measure of the heaviness of the tail of the distribution, compared to a normal distribution is the normalized fourth central moment minus 3. By this way, a normal distribution is characterized by $s = 0$ and $\kappa - 3 = 0$ and a log-normal distribution by $s_{log} = 0$ and $\kappa_{log} - 3 = 0$. The corresponding values are reported on Figures 8a, b.

The skewness, calculated on a surface-based and characterizing here the distribution of $\log(Rg)$ takes always negative values (Figure 8a), indicating a tail of the distributions on the left. This is the signature of the presence of the initial particles or small aggregates that are not destabilized and stay unchanged over time. Moreover during the aggregation phases, the absolute value of s_{log} increases because the distributions move toward larger sizes due to the floc growth but the tail characterizing the small aggregates still remain. Inversely, during the breakage steps, the modulus of s_{log}

Table 3. Fitting of the Experimental Distributions: (a) Log-Normal Distributions of the Radius of Gyration; (b) Normal Distributions of the Circularity

(a) $\frac{dF}{d\log Rg} = \frac{1}{\log(\sigma_{Rg})\sqrt{2\pi}} \exp\left(- \frac{\left(\log\left(Rg/\mu_{Rg}\right)\right)^2}{2\log(\sigma_{Rg})^2} \right)$

	Run 1 G=280 s^{-1}		Run 2 G=190 s^{-1}	
	μ_{Rg}	σ_{Rg}	μ_{Rg}	σ_{Rg}
S1	108.85	1.52	109.95	1.49
S2	49.40	1.49	64.07	1.51
S3	92.76	1.58	87.35	1.52
S4	46.06	1.49	59.14	1.49
S5	92.76	1.58	78.26	1.51

(b) $\frac{dF}{dCi} = \frac{1}{\sigma_{Ci}\sqrt{2\pi}} \exp\left(- \frac{(Ci-\mu_{Ci})^2}{2\sigma_{Ci}^2} \right)$

	Run 1 G=280 s^{-1}		Run 2 G=190 s^{-1}	
	μ_{Ci}	σ_{Ci}	μ_{Ci}	σ_{Ci}
S1	0.57	0.12	0.59	0.11
S2	0.70	0.10	0.68	0.10
S3	0.59	0.12	0.62	0.11
S4	0.71	0.09	0.69	0.10
S5	0.59	0.12	0.64	0.11

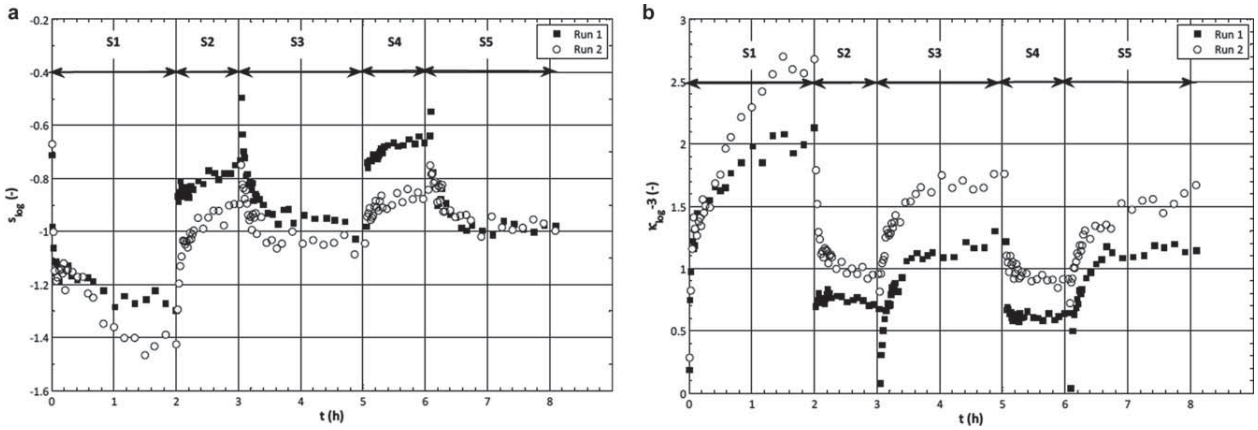

Figure 8. (a) Skewness of *Rg* distributions over time. (b) Excess kurtosis of *Rg* distributions over time.

decreases, the distribution moves toward the left and becomes more symmetric. Simultaneously, the excess kurtosis has positive values (Figure 8b) revealing the heaviness of the tail of the distribution, once again due to the presence of the small passive sub-population.

Considering the circularity distributions, the skewness and the excess kurtosis, calculated on a surface basis have been reported on Figures 9a, b. The skewness (Figure 9a) which has initially a positive value decreases over time. It expresses the presence of a tail on the right side corresponding to the primary particles or small flocs which have a high circularity. Their proportion decreases due to the aggregation mechanism and hence the skewness decreases. The excess kurtosis is always negative (Figure 9b), characterizing rather large and flat distributions. During the breakage steps S2 and S4, the skewness takes negative values during the breakage steps, indicating a tail on the left of the circularity distributions. The absolute value of the excess kurtosis decreases so the circularity distributions become less flat. The variety of shapes is more important during the re-flocculation steps S3 and S5. While the excess kurtosis is quite similar, the skewness differs significantly between the two runs. For the Run 1, the skewness gets positive value, indicating a tail on the right part of the distribution; the small flocs, produced in a high proportion, having a higher circularity. For the Run 2, the absolute value of the skewness is lower than during the breakage steps, showing that the distributions becomes more symmetric but the skewness still remains negative. Larger are the flocs, less circular they are and their presence is detected on the queue at the left of the distributions. So, the soft conditions imposed during the breakage steps of the Run 2 ($\langle G \rangle = 190\ s^{-1}$) induce a better homogeneity of shapes during the re-flocculation steps than for the Run 1 ($\langle G \rangle = 280\ s^{-1}$).

The analysis of variables such as the relative standard deviation, the skewness and the excess kurtosis gives an interesting complementary information to the one of the full distributions. Indeed, it has been seen here that nearly all the information on the change under hydrodynamic conditions of the full distributions over time is contained within these three variables. The main advantage of this analysis is that the knowledge of the first moments of the distribution, and not the distribution itself, is needed to interpret the effect of any parameter on the flocculation mechanism. The interest of this approach is in the modeling of the flocculation process based on bidimensional population balance and solving it using a method of moments.

However a limitation of this analysis is when the population distribution is multimodal, as with the number-based size distribution reported above. The interpretation of the specific

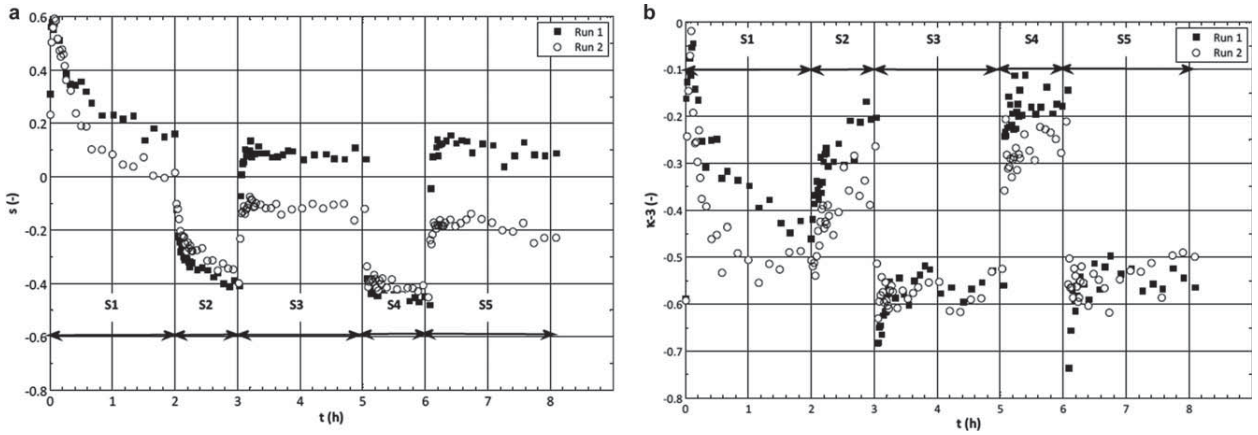

Figure 9. (a) Skewness of *Ci* distributions over time. (b) Excess kurtosis of *Ci* distributions over time.

variables, such as the relative standard deviation, the skewness and the kurtosis is much more complex.

Conclusion

This article reports experimental results of bentonite flocculation performed under controlled turbulent conditions applying successive cycles of aggregation and breakage. The different cycle sequences corresponding to preponderant aggregation or breakage mechanisms can easily be distinguished on the change of the cumulated floc number or the cumulated perimeter. The total area does not change a lot over the sequence. It can express a slight change of the internal porosity of flocs.

The change over the cycle sequence of the circularity and the radius of gyration have been analyzed both on the number-based and surface-based distributions which give complementary information. Indeed, unlike the surface-based distributions which put more in evidence the biggest aggregates, the number-based distributions are more representative of the whole population of flocs, but they may include a measurement bias since the particles having a size less than 10 pixels are not taken into account.

The number-based distributions of the radius of gyration are bimodal; they involve the signature of an inert population of primary particles and a second population of flocs (or flocculi) whose mode changes based on the cycle sequence performed at a low or high shear rate. On the contrary, the surface-based distributions are monomodal, characteristic of the population of flocs or flocculi mode changing according to the shear rate applied. Both the number-based and surface-based distributions only have one mode; the different populations of flocs distinguishable by their size present a wide variety of shapes.

The breakage steps produce flocculi whose size is calibrated by the hydrodynamics. These small flocs, more dense than the initial aggregates formed, serve then as bricks to form larger flocs during the next aggregation step. For this reason, the restructuring phenomena usually observed maintaining a constant shear rate during a flocculation process is no more present after the first cycle during a sequenced run. So, after the first breakage step, a stronger correlation appears then between the size and the shape of flocs over the following cycle sequence, whatever the step (breakage or aggregation) at steady state and during the transitory state as well. Finally a full reversibility on both floc size and shape can be reached after one or two cycles depending on the shear rate applied.

Moreover, the change over time of the size and shape of flocs can also be expressed looking at some relevant moments, especially those used for the calculation of the mean, the standard deviation, the skewness and the excess kurtosis. This approach may be particularly useful for modeling purposes based on population balance models. Indeed, once more than one property has to be considered, such as the radius of gyration and the circularity in the present case, or even more relevant floc properties, such as the area and the perimeter, the moment based methods to solve the population balance equations may be fruitful.

Literature Cited

1. Tang S, Preece JM, McFarlane CM, Zhang Z. Fractal morphology and breakage of DLCA and RLCA aggregates. *J Colloid Interface Sci*. 2000;221(1):114–123. ISSN 0021-9797. doi:10.1006/jcis.1999.6565.
2. Sorensen CM. Light scattering by fractal aggregates: a review. *Aerosol Sci Technol*. 2001;35(2):648–687. ISSN 0278-6826. doi:10.1080/02786820117868.
3. Berka M, Rice JA. Relation between aggregation kinetics and the structure of kaolinite aggregates. *Langmuir* 2005;21(4):1223–1229. ISSN 0743-7463. doi:10.1021/la0478853.
4. Ehrl L, Soos M, Morbidelli M. Dependence of aggregate strength, structure, and light scattering properties on primary particle size under turbulent conditions in stirred tank. *Langmuir* 2008;24(7):3070–3081. ISSN 0743-7463. doi:10.1021/la7032302.
5. Soos M, Moussa AS, Ehrl L, Sefcik J, Wu H, Morbidelli M. Effect of shear rate on aggregate size and morphology investigated under turbulent conditions in stirred tank. *J Colloid Interface Sci*. 2008;319(2):577–589. ISSN 0021-9797. doi:10.1016/j.jcis.2007.12.005.
6. Frappier G, Lartiges BS, Skali-Lami S. Floc cohesive force in reversible aggregation: A couette laminar flow investigation. *Langmuir*. 2010;26(13):10475–10488. ISSN 0743-7463. doi: 10.1021/la9046947.
7. Chakraborti RK, Atkinson JF, Van Benschoten JE. Characterization of alum floc by image analysis. *Environ Sci Technol*. 2000;34(18):3969–3976. doi:10.1021/es990818o.
8. Amaral AL, Ferreira EC. Activated sludge monitoring of a wastewater treatment plant using image analysis and partial least squares regression. *Analytica Chimica Acta*. 2005;544(1–2):246–253. ISSN 0003-2670. doi: 10.1016/j.aca.2004.12.061.
9. Mesquita DP, Dias O, Amaral AL, Ferreira EC. Monitoring of activated sludge settling ability through image analysis: validation on full-scale wastewater treatment plants. *Bioprocess Biosyst Eng*. 2009;32(3):361–367. ISSN 1615-7605. doi: 10.1007/s00449-008-0255-z.
10. De Temmerman P-J, Van Doren E, Verleysen E, Van der Stede Y, Abi M, Francisco D, Mast J. Quantitative characterization of agglomerates and aggregates of pyrogenic and precipitated amorphous silica nanomaterials by transmission electron microscopy. *J Nanobiotechnol*. 2012;10:24. ISSN 1477-3155. doi:10.1186/1477-3155-10-24. PMID: 22709926 PMCID: PMC3462150.
11. Allen T. *Particle Size Measurement*. New York: Chapman and Hall, 1981. ISBN 9780412154102.
12. Gorczyca B, Ganczarczyk J. Image analysis of alum coagulated mineral suspensions. *Environ Technol*. 1996;17(12):1361–1369. ISSN 0959-3330. doi:10.1080/09593331708616505.
13. Rahmani NHG, Dabros T, Masliyah JH. Fractal structure of asphaltene aggregates. *J Colloid Interface Sci*. 2005;285(2):599–608. ISSN0021-9797. doi:10.1016/j.jcis.2004.11.068.
14. Spicer PT, Pratsinis SE. Shear-induced flocculation: the evolution of floc structure and the shape of the size distribution at steady state. *Water Res*. 1996;30(5):1049–1056. ISSN 0043-1354. doi:10.1016/0043-1354(95)00253-7.
15. Biggs A, Lant PA. Activated sludge flocculation: on-line determination of floc size and the effect of shear. *Water Research*. 2000;34(9):2542–2550. ISSN 0043-1354. doi:10.1016/S0043-1354(99)00431-5.
16. Serra T, Casamitjana X. Effect of the shear and volume fraction on the aggregation and breakup of particles. *AIChE J*. 1998;44(8):1724–1730. ISSN 1547-5905. doi:10.1002/aic.690440803.
17. Jarvis P, Jefferson B, Gregory J, Parsons SA. A review of floc strength and breakage. *Water Res*. 2005;39(14):3121–3137. ISSN 0043-1354. doi:10.1016/j.watres.2005.05.022.
18. Coufort C, Bouyer D, Liné A. Flocculation related to local hydrodynamics in a Taylor–Couette reactor and in a jar. *Chem Eng Sci*. 2005;60(8–9):2179–2192. ISSN 0009-2509. doi:10.1016/j.ces.2004.10.038.
19. Bouyer D, Escudié R, Liné A. Experimental analysis of hydrodynamics in a jar-test. *Process Safet Environ Protect*. 2005;83(1):22–30. ISSN 0957-5820. doi:10.1205/psep.03109.
20. Spicer PT, Pratsinis SE, Raper J, Amal R, Bushell G, Meesters G. Effect of shear schedule on particle size, density, and structure during flocculation in stirred tanks. *Powder Technol*. 1998;97(1):26–34. ISSN 0032-5910. doi:10.1016/S0032-5910(97)03389-5.
21. Bouyer D, Liné A, Cockx A, Do-Quang Z. Experimental analysis of floc size distribution and hydrodynamics in a jar-test. *Chem Eng Res Des*. 2001;79(8):1017–1024. ISSN 0263-8762. doi:10.1205/02638760152721587.
22. Selomulya C, Amal R, Bushell G, Waite TD. Evidence of shear rate dependence on restructuring and breakup of latex aggregates. *J Colloid Interface Sci*. 2001;236(1):67–77. ISSN 0021-9797. doi:10.1006/jcis.2000.7372.
23. Hopkins DC, Ducoste JJ. Characterizing flocculation under heterogeneous turbulence. *J Colloid Interface Sci*. 2003;264(1):184–194. ISSN0021-9797. doi:10.1016/S0021-9797(03)00446-6.
24. Bubakova P, Pivokonsky M, Filip P. Effect of shear rate on aggregate size and structure in the process of aggregation and at steady

state. *Powder Technol*. 2013;235:540–549. ISSN 0032-5910. doi: 10.1016/j.powtec.2012.11.014.
25. François RJ. Strength of aluminium hydroxide flocs. *Water Research*. 1987;21(9):1023–1030. ISSN 0043-1354. doi: 10.1016/0043-1354(87)90023-6.
26. Bouyer D, Coufort C, Liné A, Do-Quang Z. Experimental analysis of floc size distributions in a 1-l jar under different hydrodynamics and physicochemical conditions. *J Colloid Interface Sci*. 2005; 292(2):413–428. ISSN 0021-9797. doi:10.1016/j.jcis.2005.06.011.
27. Coufort C, Dumas C, Bouyer D, Liné A. Analysis of floc size distributions in a mixing tank. *Chem Eng Process Process Intensif*. 2008; 47(3):287–294. ISSN 0255-2701. doi:10.1016/j.cep.2007.01.009.
28. Barbot E, Dussouillez P, Bottero J-Y, Moulin P. Coagulation of bentonite suspension by polyelectrolytes or ferric chloride: floc breakage and reformation. *Chem Eng J*. 2010;156(1):83–91. ISSN 1385-8947. doi:10.1016/j.cej.2009.10.001.
29. Li T, Zhu Z, Wang D, Yao C, Tang H. The strength and fractal dimension characteristics of alum–kaolin flocs. *Int J Mineral Process.* 2007; 82(1):23–29. ISSN 0301-7516. doi:10.1016/j.minpro.2006.09.012.
30. Wang Y, Gao B-Y, Xu X-M, Xu W-Y, Xu G-Y. Characterization of floc size, strength and structure in various aluminum coagulants treatment. *J Colloid Interface Sci*. 2009;332(2):354–359. ISSN 0021-9797. doi:10.1016/j.jcis.2009.01.002.
31. Xiao F, Lam KM, Li XY, Zhong RS, Zhang XH. PIV characterisation of flocculation dynamics and floc structure in water treatment. *Colloid Surfaces A Physicochem Eng Asp*. 2011;379(1–3):27–35. ISSN 0927-7757. doi:10.1016/j.colsurfa.2010.11.053.
32. He W, Nan J, Li H, Li S. Characteristic analysis on temporal evolution of floc size and structure in low-shear flow. *Water Res*. 2012;46(2):509–520. ISSN 0043-1354. doi:10.1016/j.watres.2011.11.040.
33. Hofmann U, Endell K, Wilm D. Kristallstruktur und Quellung von Montmorillonit (Das Tonmineral der Bentonittone.) *Z Kristallogr*. 1933;86:340–348.
34. Duan J, Gregory J. Coagulation by hydrolysing metal salts. *Advances in Colloid and Interface Science*. 2003;100/102:475–502. ISSN 0001-8686. doi: 10.1016/S0001-8686(02)00067-2.
35. Wendt F. Turbulente Strömungen zwischen zwei rotierenden konaxialen Zylindern. *Ing Arch*. 1933;4:577–595. doi:10.1007/BF02084936.
36. Vlieghe M, Coufort-Saudejaud C, Frances C, Liné A. *In situ* characterization of floc morphology by image analysis in a turbulent Taylor–Couette reactor. *AIChE J*. 2014;60(7):2389–2403. ISSN 1547-5905. doi:10.1002/aic.14431.